Crystallization via shaking in a granular gas with van der Waals interactions

Qiong Bai[1] and Marco G. Mazza[1,2]

[1]*Max Planck Institute for Dynamics and Self-Organization (MPIDS), D-37077 Göttingen, Germany*

[2]*Interdisciplinary Centre for Mathematical Modelling and Department of Mathematical Sciences, Loughborough University, Loughborough, Leicestershire LE11 3TU, United Kingdom*

(Received 19 August 2018; published 31 October 2019)

We investigate the effect of van der Waals forces on a collection of granular particles by means of molecular dynamics simulations of a vibrated system in three dimensions. The van der Waals interactions introduce two phase coexistences: one between a random close packing and a gas and a second between a polycrystalline dense state and a gas, where the dense, disordered component crystallizes when the driving amplitude exceeds a threshold value. The region of stability of the ordered state in the nonequilibrium phase diagram grows in size as the Hamaker constant increases or the degree of dissipation increases.

DOI: 10.1103/PhysRevE.100.042910

The collective behavior of granular matter remains a major challenge in physics [1–3]. Despite the deceptive simplicity of particulate interactions—dissipative and frictional contacts—a myriad of complex phenomena have been recognized, for example, pattern formation [4], clustering [5–7], Rayleigh-Bénard convection [8,9], and nonequilibrium phase transitions [10–12].

While considerable efforts have been focused to discover the consequences of granular contact forces, much less attention has been devoted to study transitions induced by noncontact interactions, such as the van der Waals force. This force is ubiquitous, due to its origin in the fluctuations of electronic charge density [13], and it becomes relevant for particles' diameters $1\ \mu\text{m} \leqslant d \leqslant 100\ \mu\text{m}$ [14–17].

Interesting mesoscopic and macroscopic collective effects are known in powders technologies [14,18–20], and van der Waals forces have been recognized to be crucial from geckos' climbing ability [21,22] to the structural cohesion of a class of asteroids [17,23,24].

Here we report on molecular dynamics (MD) simulations of a granular system, consisting of spherical particles of diameter $d = 70\ \mu\text{m}$ and density $\rho = 8.9\ \text{g/cm}^3$ (corresponding to bronze). All particles are confined in the z direction by two walls separated by a distance L_z, and the whole system is vibrated sinusoidally with amplitude A and frequency ν along the z direction. The simulated domain has dimensions $L_x = 160d$, $L_y = 20.0d$, $L_z = 18.5d$, and periodic boundary condition are used along the x and y directions. On collision, two granular particles will dissipate energy. The energy dissipation is quantified by the restitution coefficient ϵ, which is the ratio of the relative speed between the particles after the collision to the same quantity before the collision. Here we neglect both tangential forces and the tangential coefficient of restitution.

Newton's second law of motion can be used to describe the motion of individual particles. The governing equations for particle i with mass m can be written as

$$m\frac{d\boldsymbol{v}_i}{dt} = \sum_j \boldsymbol{f}^c_{ij} + \sum_k \boldsymbol{f}^{\text{nc}}_{ik} + \boldsymbol{f}^w_i, \tag{1}$$

where $\boldsymbol{v}_i$ is the velocity, $\boldsymbol{f}^c_{ij}$ is the contact force on particle i due to particle j, $\boldsymbol{f}^{\text{nc}}_{ik}$ is the noncontact force acting on particle i due to particle k, and $\boldsymbol{f}^w_i$ is the force imposed by the wall.

The contact force between particles is [25]

$$\boldsymbol{f}^c_{ij} = \Theta(d - |\boldsymbol{r}_{ij}|)[-k(d - |\boldsymbol{r}_{ij}|) + \mu \boldsymbol{v}_{ij} \cdot \hat{\boldsymbol{r}}_{ij}]\hat{\boldsymbol{r}}_{ij}, \tag{2}$$

where k is the spring constant, μ the damping coefficient, $\boldsymbol{r}_{ij} \equiv \boldsymbol{r}_j - \boldsymbol{r}_i$, $\boldsymbol{v}_{ij} \equiv \boldsymbol{v}_j - \boldsymbol{v}_i$, and $\Theta(x)$ is the Heaviside step function. The Hamaker theory for mesoscopic bodies is used here to calculate the van der Waals force [16,26],

$$\boldsymbol{f}^{\text{nc}}_{ij} = -\Theta(h)\frac{Hd}{24h^2}\hat{\boldsymbol{r}}_{ij}, \tag{3}$$

where the Hamaker constant H depends on geometry and material properties and $h = |\boldsymbol{r}_{ij}| - d$ is the surface-to-surface separation between the grains in the normal direction. Because the force drops off rapidly with increasing separation, we ignore the van der Waals force for $h > 0.25d$ (our results in the following do not depend qualitatively on this cutoff choice). The divergence of the van der Waals force in Eq. (3) for vanishing distances derives from the macroscopic treatment of dispersion forces under which it was derived [26]; to remove this divergence, the force is cut off at $h_0 = 1$ nm [27]; for distances $h \leqslant h_0$, $\boldsymbol{f}^{\text{nc}}_{ij}(h) = \boldsymbol{f}^{\text{nc}}_{ij}(h_0)$.

The strong variation of the force at very small distances can cause numerical instabilities. These are avoided by employing a customary shifted expression for the magnitude $f^{\text{nc}}_{\text{shift}} = |\boldsymbol{f}^{\text{nc}}_{ij}|$,

$$f^{\text{nc}}_{\text{shift}} = \Theta(h)\frac{H_{\text{shift}}d}{24(h + d/c)^2}, \tag{4}$$

where $H_{\text{shift}} = \frac{5}{16}10^{10}H$ is the modified Hamaker constant, chosen so that the van der Waals potential energy associated to Eq. (4) is equal to the potential energy associated to Eq. (3), including the cutoffs, and $c = 8.0$ is a constant describing how much we shift the force with respect to the particle diameter.

The vibrating walls inject energy into the system through the collisions between particles and walls. The collision force

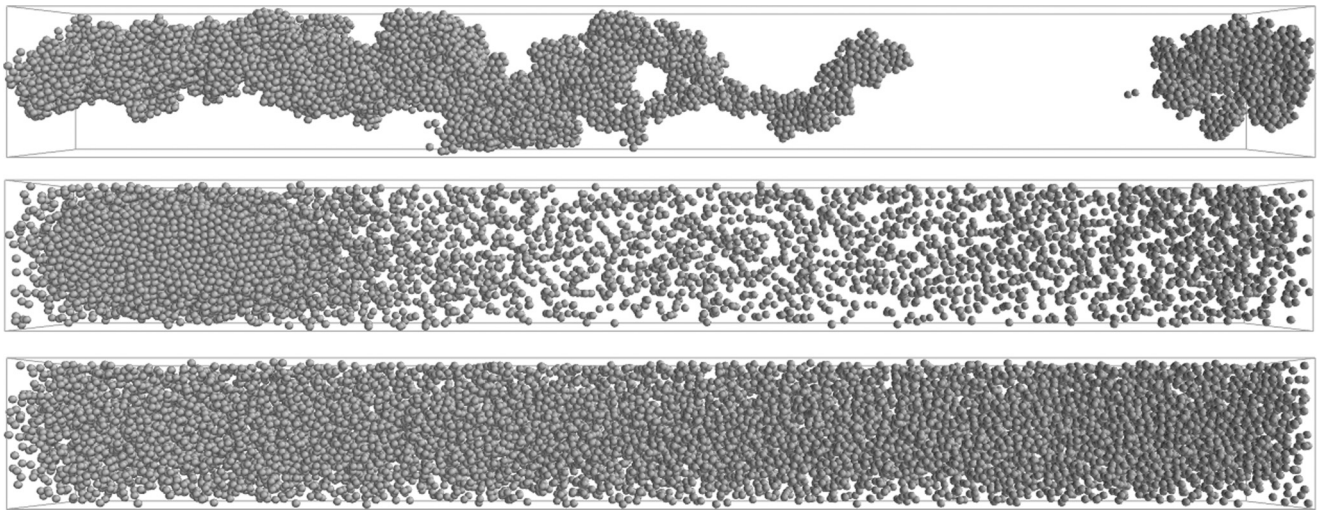

FIG. 1. Three characteristic snapshots for the system at $\bar{\phi} = 0.10$ and $A = 0.10d, 0.46d$, and $0.50d$ (from top to bottom), which correspond to the cluster, coexistence, and homogeneous state, respectively. The system is viewed laterally, while the vibration is imposed in the vertical direction.

[similarly to Eq. (2)] reads

$$\boldsymbol{f}_i^w = k\delta\zeta\Theta(\zeta)\hat{\boldsymbol{z}} + \mu(\boldsymbol{v}_w - \boldsymbol{v}_i)\cdot\hat{\boldsymbol{z}}, \tag{5}$$

where $\zeta \equiv \frac{d}{2} - |z_w - z_i|$ is the overlap between wall and particle; z_i and $\boldsymbol{v}_i$ are the z coordinate and velocity of particle i on colliding with the wall, respectively; z_w and $\boldsymbol{v}_w$ are the z coordinate and velocity of the wall; and $\delta = -1(+1)$ for the top (bottom) wall.

We solve the equation of motion [Eq. (1)] for N particles via a Verlet algorithm with a time step $\delta t = 10^{-6}$ s. All our simulations have a total runtime of $10^8\delta t$. We set the driving frequency $\nu = 50$ Hz, the restitution coefficient $\epsilon = 0.9$ and $H = 8.0 \times 10^{-20}$ J if not specified otherwise. The spring constant $k = 0.5$ N/m for both particle-particle and particle-wall collisions, while the damping coefficient μ is determined by k and ϵ.

We map the nonequilibrium phase diagram by varying the average filling fraction $\bar{\phi} \equiv \frac{N\pi d^3}{6V}$, $V = L_x L_y L_z$, and the driving amplitude A, where N is the total number of particles. Generally, we find three main regimes in our simulated phase space: (i) a clustered state, (ii) a coexistence between solidlike and gas, and (iii) a homogeneous state. Figure 1 shows representative snapshots for each state. In the clustered state, nearly all particles belong to a system spanning, solidlike cluster. In the coexistence state, the system separates along the x direction into a dense, solidlike region and a dilute, gaslike one. In the homogeneous state, the system is translationally invariant with a gaslike or liquidlike density (see below for a discussion of the difference).

The phase diagram of our cohesive granular system is shown in Fig. 2. We first summarize the main features of the phase diagram. At very low driving amplitude A, the energy injection into the system is too weak to overcome the combined effect of attractive van der Waals forces and dissipation, and all particles stick together, thus forming a large cluster. On increasing A, the system spontaneously separates, and we find a coexistence between a random close packing (RCP) and gas (G) state. At slightly larger A, we observe a second coexistence state, namely between a polycrystal (PC) and gas phase. Outside of the stability region of these coexistence states, the cluster state turns to liquid as A grows, at large $\bar{\phi}$, while the system reaches a homogeneous gas state at large A and small $\bar{\phi}$.

To precisely characterize the observed states, we consider the following observables: the radial distribution function $g(r)$, local order parameters such as the sixfold bond orientational order parameter q_6, and the coordination number Z. The radial distribution function is defined as

$$g(r) = \frac{V}{N^2}\left\langle \sum_i \sum_{j\neq i} \delta(r - r_{ij}) \right\rangle, \tag{6}$$

where $r_{ij} = |\boldsymbol{r}_{ij}|$. The coordination number Z is the average number of nearest neighbors for each particle, where the

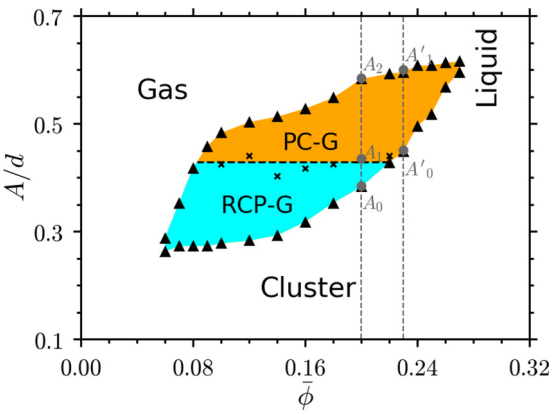

FIG. 2. The phase diagram in the space of A-$\bar{\phi}$. The black filled triangles form the spinodal line, which confines the coexistence region. When the gas coexists with a solid plug, the latter is a PC-G state in the orange shaded region and RCP-G state in the aqua region. The black crosses mark specific simulations at the boundary of RCP-G and PC-G, and the black dashed line is the fit of the boundary line. See Figs. 3 and 4 for the values of driving amplitudes marked in gray along the vertical gray lines.

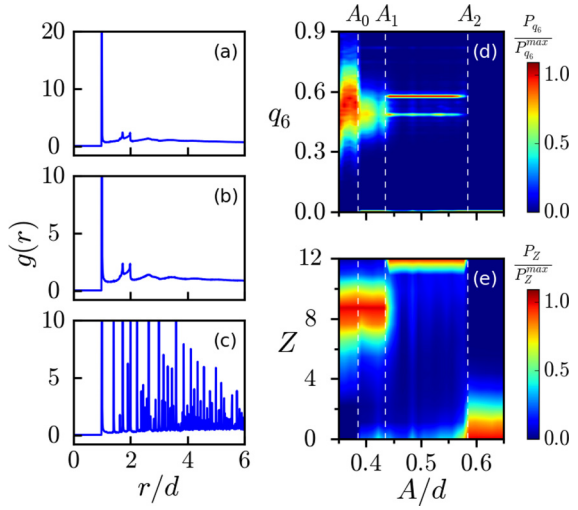

FIG. 3. Quantitative characterization of all phases for the system with $\bar{\phi} = 0.20$. Panels (a), (b), and (c) are the radial distribution functions for systems with $A = 0.36d$, $0.40d$, and $0.50d$, respectively. Panels (c) and (d) are the heat maps of the distribution of q_6 and Z for varying A/d, respectively. The amplitudes marked in (d) and (e) are $A_0 = 0.385d$, $A_1 = 0.435d$, and $A_2 = 0.585d$.

search radius for nearest neighbors $r_c = 1.01d$. q_6 is a bond orientation order parameter typically used to characterize hexagonal order [28]. For each particle i, it is defined as

$$q_l(i) = \left[\frac{4\pi}{2l+1}\sum_{m=-l}^{l}|q_{l,m}(i)|^2\right]^{1/2},$$
$$q_{l,m}(i) = \frac{1}{N_b(i)}\sum_{j=1}^{N_b(i)}Y_{l,m}(\theta_{i,j},\phi_{i,j}), \tag{7}$$

with $l = 6$. $Y_{l,m}$ are the spherical harmonics, $\theta_{i,j}$ and $\phi_{i,j}$ are the polar and azimuthal angles of center-of-mass distance vector $\boldsymbol{r}_{ij}$, and $N_b(i)$ is the number of nearest neighbors within $r_c = 1.01d$. Typical values of q_6 are 0.485 and 0.575 for hexagonal-close packing (HCP) and face-centered cubic (FCC) structures, respectively.

Figure 3 shows the calculation of $g(r)$, q_6, and Z at fixed $\bar{\phi} = 0.20$. At low A and for $A < A_0 \simeq 0.38$ the system is in the dense, clustered state, as shown by q_6 which is mainly distributed between 0.32 and 0.7 [Fig. 3(d)] and Z which ranges in the interval [7, 10] [Fig. 3(e)]. The $g(r)$ plot [Fig. 3(a)] shows an interesting splitting of the second main peak at $\sqrt{3}d$ into two small peaks at $\sqrt{2}d$ and $\sqrt{3}d$; this is a signature of RCP structure [29,30].

For driving amplitudes $A_0 < A < A_1 \simeq 0.44$, the system shows evidence of the coexisting between RCP and G states. The $g(r)$ [Fig. 3(b)] and Z distribution appear similar to the low-A clustered state. However, the q_6 distribution distinctly narrows down to the interval [0.4, 0.6] for the RCP component while another peak arises at $q_6 = 0.0$ for the gas component. On further increase of the amplitude, and for $A_1 < A < A_2 \simeq 0.58$, clear signatures of PC-G coexistence appear. Numerous peaks arise in the $g(r)$ [Fig. 3(c)] and Z has mainly a bimodal distribution peaked near 12 and 0. The bond orientational order parameter, beside the peak at 0.0, shows another two peaks at $q_6 = 0.485$ and 0.575, which are clear evidence of the

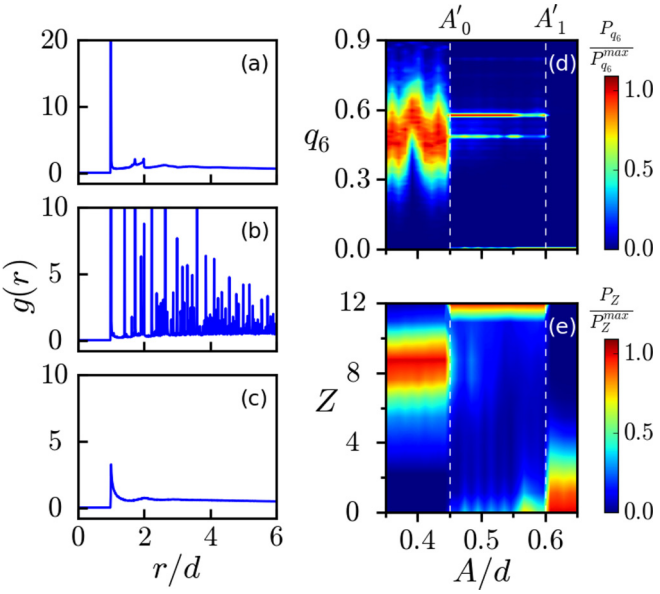

FIG. 4. Quantitative characterization of all phases for the system with $\bar{\phi} = 0.23$. Panels (a), (b), and (c) are the radial distribution functions for systems with $A = 0.40d$, $0.50d$, and $0.60d$, respectively. Panels (d) and (e) are the heat maps of the distribution of q_6 and Z for varying A/d, respectively. The amplitudes marked in (d) and (e) are $A'_0 = 0.45d$ and $A'_1 = 0.60d$, respectively.

presence of both HCP and FCC structures. Above $A_2 \simeq 0.57$, the system is in a liquidlike state, characterized by $q_6 \simeq 0$ and Z ranging from 0 to 2.

Figure 4 shows calculations along another path on the A-$\bar{\phi}$ phase diagram (Fig. 2) at $\bar{\phi} = 0.23$. Similarly to the case at $\bar{\phi} = 0.20$, the system exhibits a PC-G state for $A'_0 < A < A'_1$, $A'_0 \simeq 0.45$, $A'_1 \simeq 0.6$. Unlike the case for $\bar{\phi} = 0.20$, however, the system transitions directly from the clustered state to the PC-G state because of the spinodal line delimiting the end of the RCP-G coexistence at large filling fractions.

In Fig 5, we show a snapshot of the PC-G state, where each particles is color-coded according to its value of q_6. Particles in the gas state are mainly blue with $q_6 = 0.0$ or 1.0. Inside the solid plug, particles have mainly two types of local structures. The first one is HCP with q_6 around 0.485 (particles colored in light green) and the other one is FCC with q_6 around 0.575 (colored in yellow-green). Unlike the results in Ref. [30] the crystalline structures observed in our system do not have a preferential orientation, such as parallel or perpendicular to the walls. We have also verified that, once formed, the PC structures are irreversible and remain stable even on

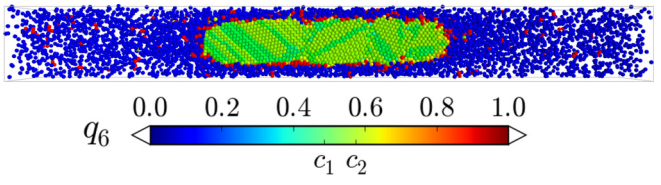

FIG. 5. The steady-state snapshot of system with $\bar{\phi} = 0.20$ and $A = 0.55d$. The particle are color coded according to the local q_6 number. c_1, c_2 are 0.485 and 0.575, marking the HCP and FCC structures, respectively.

quenching A down to within the RCP-G coexistence region. We now ask the question: What determines the boundary between the RCP-G domain and PC-G domain?

We find it useful to follow the system's dynamics in terms of its energy. As we start our simulations from a homogeneous granular gas (of interest in microgravity conditions [31,32]) we consider the balance of energy injected by the walls and dissipated by collisions. We find that the transient path of the system is governed by the typical energy associated to the vibrating walls, collisional dissipation, and the typical cohesive energy due to van der Waals interactions. The ultimate steady state reached by the system is determined by the above energy scales.

Starting from a homogeneous, dilute initial condition, the system effectively experiences a moderate granular cooling process before phase separating due to the driving. For $A \leqslant L_g/\pi$, where L_g is the system clearance (the difference between box height and the thickness of the RCP plug), the system is in the gaslike state [33]. Hence, the dissipation rate during the cooling process is

$$e_{\text{diss}} = f_{\text{coll}}(1-\epsilon^2), \tag{8}$$

where f_{coll} is the collision frequency. The energy injection rate increases linearly with the amplitude A.

The energy ratio $\mathcal{E}$ between the energy injection rate e_{inj} and the energy dissipation rate e_{diss} can therefore be written as

$$\mathcal{E} \propto \frac{A}{1-\epsilon^2}. \tag{9}$$

Granular collisions and van der Waals cohesion combined produce a "dissipative trap," where particles with low-enough kinetic energy stick together at the collision point and form disordered clusters. Organization into a regular, crystalline structure is possible if the grains have sufficient energy to escape this dissipative trap. Thus, we expect that above a certain threshold amplitude $A^* \equiv A^*(H)$, dependent on the Hamaker constant H, the PC state is possible.

We find that, once the steady state is reached, the ratio of characteristic energies $\mathcal{E}^* \propto A^*/(1-\epsilon^2)$ determines the steady-state boundary between RCP-G state and PC-G state.

Figure 6 shows the dependence of the boundary line between the RCP-G state and the PC-G state on the dissipation coefficient $1-\epsilon$ from our simulation results with a fixed Hamaker constant. The transition value A^* converges to 0 as $\epsilon \to 1.0$, which indicates that the phase separation is a granular effect. The fit to the data is in good agreement with $\mathcal{E}^* = \text{const}$, which supports the picture that a characteristic value of $\mathcal{E}$ is required to turn the RCP-G state into a PC-G state. This should be physically linked to the nucleation barrier of the crystalline states. However, this kind of analysis is prohibitive in our granular system, so we cannot directly probe the nucleation barrier. For increasing dissipation $(1-\epsilon)$, stronger driving amplitudes are then necessary to overcome the dissipative "trap" and lead to reorganization into a crystalline structure. Interestingly, in analogy to the quenching of an equilibrium liquid, we find that very rapid cooling may avoid the crystallization and result in a metastable RCP state.

According to our results, the solid-gas phase separation shown by a vibrated granular system with van der Waals interactions does not exist in a granular system with only head-on collisions. That is, the van der Waals interaction is another prerequisite for the present phase separation. The attractive interactions trap the particles with energy below a material-dependent threshold. This would imply that stronger attractive forces should increase the domain of stability of the PC-G state. Figure 7 confirms this expectation. We show the phase boundaries in the space of Hamaker constant and A. For a given material, there will be a corresponding interval of A where the system shows a PC-G state. As the Hamaker constant increases, i.e., the attractive strength increases, the PC-G state regime will expand and shift to higher driving values. Conversely, for decreasing Hamaker constant, the threshold values of the phase boundaries converge to zero.

The significance of the results in Fig. 7 is that for a given material we can estimate the driving energy necessary for spontaneous crystallization. While in the results presented

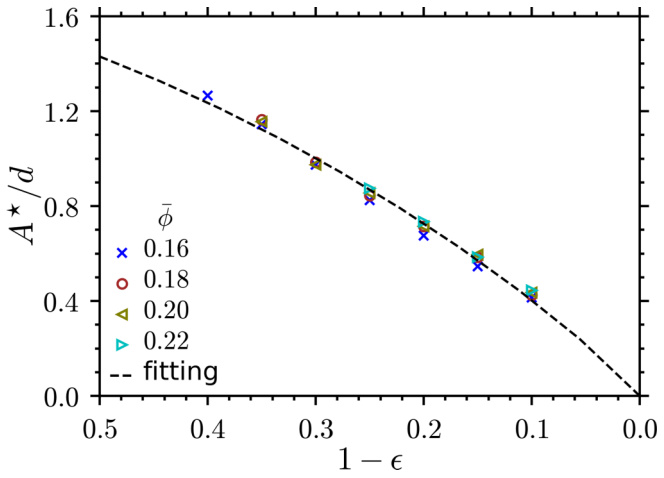

FIG. 6. Dependence of the threshold amplitude A^* between RCP-gas and PC-gas coexistence states on the coefficient of restitution ϵ. All symbols are simulation results, and different colors correspond to different filling fractions $\bar{\phi}$. The dashed line is the fit to the function $A^*/d = c_1(1-\epsilon^2)^{c_2}$ with $c_1 = 1.86$ and $c_2 = 0.92$.

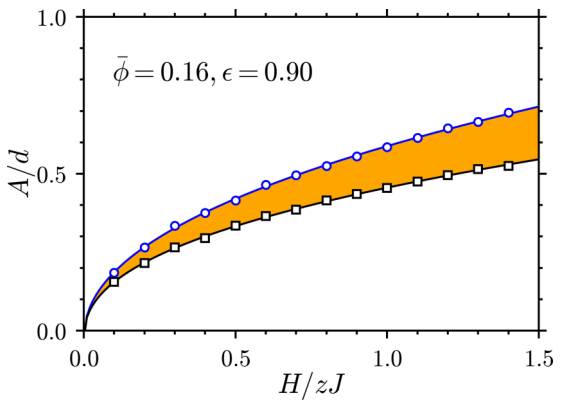

FIG. 7. The phases boundaries in the space of H-A^* for system with $\bar{\phi} = 0.16$ and $\epsilon = 0.9$ (1 zJ $= 10^{-21}$ J). The orange shaded region is where the system is in the PC-G state. Blue circles mark the boundary between the homogeneous state and PC-G state. The black squares marks the boundary between the PC-G state and RCP-G state. Circles and squares are from simulation data and the solid lines are fits to the functions $A^*/d = c_0 + c_1 H^{c_2}$, $A^*/d = c_0 + c_3 H^{c_4}$ with $c_0 \approx 0$, $c_1 = 0.62$, $c_2 = 0.46$, $c_3 = 0.48$, and $c_4 = 0.42$.

here gravity is absent, we have verified that for accelerations $g = 10^{-4}$ m/s^2 the phase diagram is qualitatively unchanged.

In summary, we find that cohesive, van der Waals forces induce a novel phase coexistence in a granular gas system under gentle driving. For moderate shaking strength, the cluster is randomly packed, whereas for higher input energies the cluster becomes crystalline. We identify that the combination of dissipation and cohesion are necessary to observe these phases. These findings might be useful not only to the granular community but also to the larger field of out-of-equilibrium disordered media.

We are grateful to Annette Zippelius, Matthias Schröter, Stephan Herminghaus for stimulating discussions and to an anonymous referee for helpful input. We thank Thomas Eggers for technical support and the Max Planck Society for funding. We gratefully acknowledge the computational time on JURECA at the Jülich Supercomputing Centre.

[1] H. M. Jaeger, S. R. Nagel, and R. P. Behringer, Rev. Mod. Phys. **68**, 1259 (1996).
[2] J. Rajchenbach, Adv. Phys. **49**, 229 (2000).
[3] I. S. Aranson and L. S. Tsimring, Rev. Mod. Phys. **78**, 641 (2006).
[4] P. B. Umbanhowar, F. Melo, and H. L. Swinney, Nature **382**, 793 (1996).
[5] I. Goldhirsch and G. Zanetti, Phys. Rev. Lett. **70**, 1619 (1993).
[6] M. Hummel, J. P. Clewett, and M. G. Mazza, Europhys. Lett. **114**, 10002 (2016).
[7] M. Hummel and M. G. Mazza, Phys. Rev. E **93**, 022905 (2016).
[8] J. R. de Bruyn, C. Bizon, M. D. Shattuck, D. Goldman, J. B. Swift, and H. L. Swinney, Phys. Rev. Lett. **81**, 1421 (1998).
[9] P. Eshuis, D. van der Meer, M. Alam, H. J. van Gerner, K. van der Weele, and D. Lohse, Phys. Rev. Lett. **104**, 038001 (2010).
[10] M. Argentina, M. G. Clerc, and R. Soto, Phys. Rev. Lett. **89**, 044301 (2002).
[11] M. G. Clerc, P. Cordero, J. Dunstan, K. Huff, N. Mujica, D. Risso, and G. Varas, Nat. Phys. **4**, 249 (2008).
[12] K. Roeller, J. P. D. Clewett, R. M. Bowley, S. Herminghaus, and M. R. Swift, Phys. Rev. Lett. **107**, 048002 (2011).
[13] J. Hermann, R. A. DiStasio, Jr, and A. Tkatchenko, Chem. Rev. **117**, 4714 (2017).
[14] F. J. Muzzio, T. Shinbrot, and B. J. Glasser, Powder Technol. **124**, 1 (2002).
[15] A. Castellanos, Adv. Phys. **54**, 263 (2005).
[16] H. P. Zhu, Z. Y. Zhou, R. Y. Yang, and A. B. Yu, Chem. Eng. Sci. **62**, 3378 (2007).
[17] D. J. Scheeres, C. M. Hartzell, P. Sánchez, and M. Swift, Icarus **210**, 968 (2010).
[18] J. Visser, Powder Technol. **58**, 1 (1989).
[19] F. F. Lange, J. Am. Ceram. Soc. **72**, 3 (1989).
[20] Q. Li, V. Rudolph, B. Weigl, and A. Earl, Int. J. Pharm. **280**, 77 (2004).
[21] K. Autumn, Y. A. Liang, S. T. Hsieh, W. Zesch, W. P. Chan, T. W. Kenny, R. Fearing, and R. J. Full, Nature **405**, 681 (2000).
[22] K. Autumn, M. Sitti, Y. A. Liang, A. M. Peattie, W. R. Hansen, S. Sponberg, T. W. Kenny, R. Fearing, J. N. Israelachvili, and R. J. Full, Proc. Natl. Acad. Sci. U.S.A. **99**, 12252 (2002).
[23] B. Rozitis, E. MacLennan, and J. P. Emery, Nature **512**, 174 (2014).
[24] P. Sánchez and D. J. Scheeres, Meteorit. Planet. Sci. **49**, 788 (2014).
[25] S. Luding, Phys. Rev. E **55**, 4720 (1997).
[26] H. C. Hamaker, Physica **4**, 1058 (1937).
[27] J. N. Israelachvili, *Intermolecular and Surface Forces* (Academic Press, London, 2011).
[28] P. Rein ten Wolde, M. J. Ruiz-Montero, and D. Frenkel, J. Chem. Phys. **104**, 9932 (1996).
[29] Y. Jin and H. A. Makse, Physica A **389**, 5362 (2010).
[30] A. Panaitescu, K. A. Reddy, and A. Kudrolli, Phys. Rev. Lett. **108**, 108001 (2012).
[31] K. Harth, U. Kornek, T. Trittel, U. Strachauer, S. Höme, K. Will, and R. Stannarius, Phys. Rev. Lett. **110**, 144102 (2013).
[32] K. Harth, T. Trittel, S. Wegner, and R. Stannarius, Phys. Rev. Lett. **120**, 214301 (2018).
[33] A. Sack, M. Heckel, J. E. Kollmer, F. Zimber, and T. Pöschel, Phys. Rev. Lett. **111**, 018001 (2013).